Thermodynamics and Lattice Vibrations of Minerals: 2. Vibrational Characteristics of Silicates

SUSAN WERNER KIEFFER[1]

Department of Earth and Space Sciences, University of California, Los Angeles, California 90024

General lattice vibrational properties of minerals, particularly those properties which strongly influence the thermodynamic behavior, are discussed in this paper (the second of a series relating thermodynamic and lattice vibrational properties of minerals). Infrared (IR), Raman (R), and inelastic neutron scattering (INS) data are summarized, if known, for the following minerals: halite (INS), periclase (INS), corundum (IR, R), brucite (IR, R, partial INS), quartz (R, IR, INS), cristobalite (IR, R), silica glass (IR, R, partial INS), stishovite (IR), rutile (R, IR, INS), albite (IR, R), microcline (IR), spinel (IR, R), muscovite (IR, R), jadeite (IR), diopside (IR, R), enstatite (IR, R), olivine (IR, R), zircon (IR, R), kyanite (IR), andalusite (IR), sillimanite (IR), pyrope (IR), andradite (IR), grossular (IR), and calcite (IR, R, INS). New high-resolution infrared data are given for kyanite, andalusite, sillimanite, stishovite, coesite, jadeite, diopside, pyrope, andradite, and grossular. The data presented and summarized show that optic modes of vibration of silicates are spread over a range of frequencies, generally from wave numbers as low as 75 cm^{-1} to wave numbers as high as 1200 cm^{-1}. The far-infrared (low frequency) optic modes are particularly important in this study because they strongly influence the low-temperature heat capacity and therefore the entropy. The mid-infrared (high frequency) optic modes generally arise from the vibrations of tightly bound clusters within the structures and can generally be recognized as isolated bands in the vibrational spectrum. A method is given for enumeration of the fraction of total vibrational modes which are internal stretching modes. Inelastic neutron scattering data are reviewed to show the magnitude of anisotropy and dispersion of acoustic modes and of dispersion of optic modes in the minerals. The combined infrared, Raman, and INS data show that, excluding the stretching modes of quasi-molecular clusters within the minerals, the optic modes do not appear to follow a simple recognizable distribution, such as a Debye distribution, but are rather uniformly distributed across a broad range of frequencies.

CONTENTS

1. INTRODUCTION

Infrared (IR), Raman (R), and inelastic neutron scattering (INS) spectra provide information about lattice vibrational properties. In general, all three types of spectra are required for a complete description of the lattice vibrations, because Raman or infrared spectra by themselves reveal only lattice vibrations which interact with photons under particular, restricted experimental conditions (see, for example, discussions in the work of *Farmer* [1974*a*, *b*], *Hadni* [1974], and *Karr* [1975]). Complete vibrational characterizations are available for only a few minerals, but these data allow some generalizations about mineral spectra to be made. A brief summary of existing data, with emphasis on the properties important in thermodynamic calculations, new data on the minerals of interest in this study, and a method for enumerating intramolecular cluster modes are presented here. These spectroscopic data and concepts provide the basis for a generalized thermodynamic model for minerals described in paper 3 of this series [*Kieffer*, 1979*b*].

2. MINERALS STUDIED

The minerals studied have a wide range of compositions and structures. They are listed below according to the classification of *Bragg et al.* [1965] (for silicates). This classification is convenient because it is based on the polymerization of the tetrahedral silicon-oxygen groups, a property which influences the vibrational characteristics.

1. Simple minerals and oxides studied for comparison with Debye solids are halite, corundum, spinel, stishovite, rutile, periclase, and (for comparison with periclase) brucite.
2. The framework silicates studied are quartz, cristobalite, silica glass, coesite, albite, and microcline. Stishovite and rutile will often be discussed with the framework silicates in order to provide a comparison of effects arising from fourfold and sixfold coordination of the cations.
3. The sheet and chain silicates studied are muscovite, jadeite, diopside, and enstatite.
4. The minerals containing isolated clusters studied include the orthosilicates forsterite, zircon, kyanite, andalusite, sillimanite, grossular, pyrope, and andradite and calcite with the isolated CO_3^{-2} ion.

3. DATA: MODES OBSERVED IN INFRARED, RAMAN, AND INELASTIC NEUTRON SCATTERING SPECTRA

Infrared and Raman Data

Infrared and Raman spectra provide information about the frequency of the optical lattice vibrational modes at wave vector $\mathbf{K} = 0$. Mid-infrared data ($400 < w < 4000$ cm^{-1}) are relatively abundant, Raman data are less abundant, and far-infrared data ($w < 400$ cm^{-1}) are relatively rare. Existing data for the minerals used in this thermodynamic study are summarized in Tables 1–4 (table notes are given in the appendix); new

[1] Now at U.S. Geological Survey, Flagstaff, Arizona 86001.

Paper number 8R1054.
0034-6853/79/018R-1054$06.00

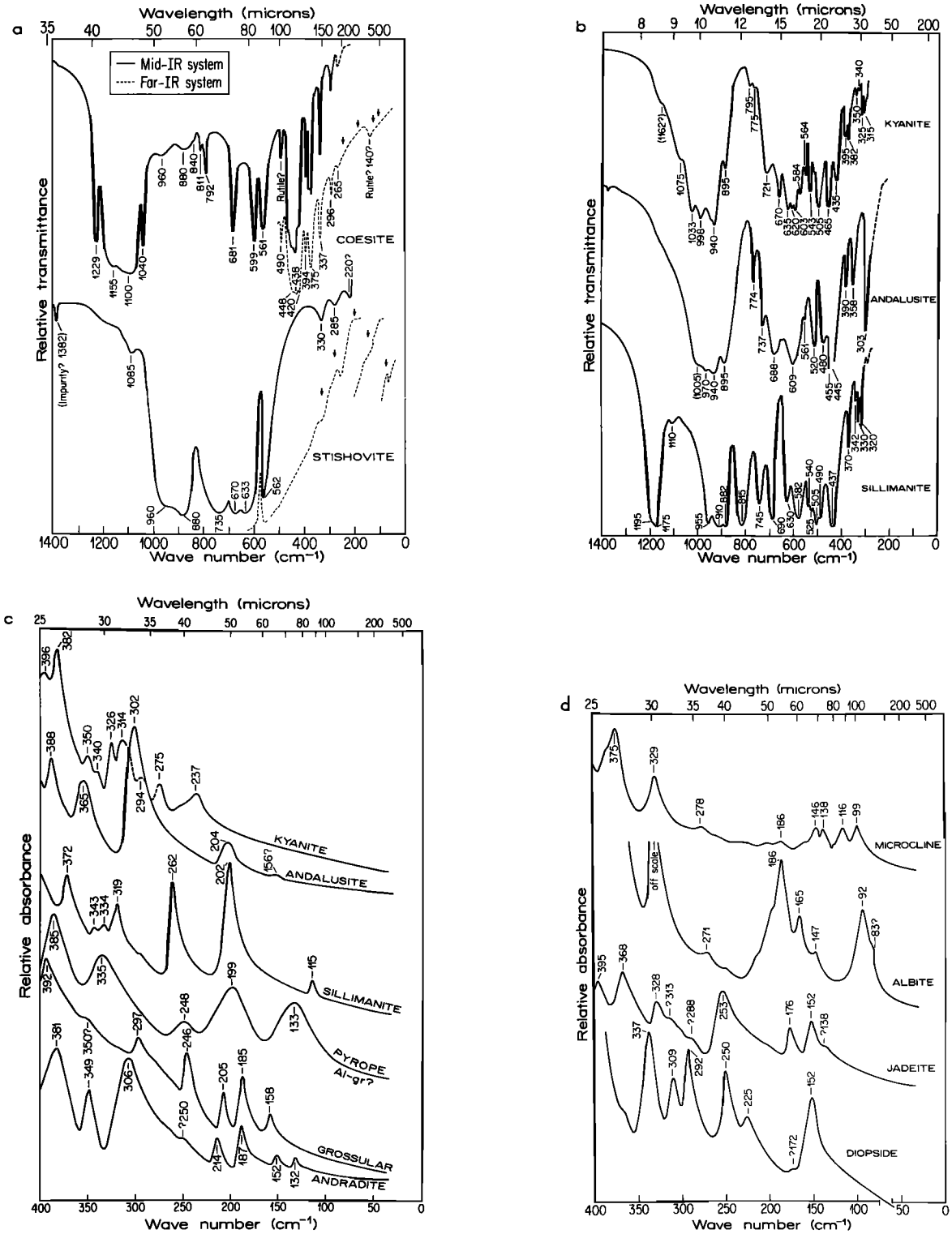

Fig. 1. (*a*) Mid-infrared and far-infrared spectra of coesite and stishovite. Spectrometer grating changes are shown by the arrows; offsets in the spectra at these points may be artifacts. The weak line at 140 cm^{-1} in the coesite spectrum could not be reproduced in other runs and is therefore probably due to an impurity. See notes to Table 2 in the appendix. (*b*) Mid-infrared spectra of the Al_2SiO_5 polymorphs. See notes to Table 4 in the appendix. (*c*) Far-infrared spectra of the Al_2SiO_5 polymorphs and three garnets. See notes to Table 4 in the appendix. (*d*) Far-infrared spectra of-microcline, albite, jadeite, and diopside. See notes to Tables 2 and 3 in the appendix.

high-resolution infrared data are shown in Figure 1. Composition and lattice constants for the minerals shown in Figure 1 are shown in Table 5. The data are for polycrystalline samples unless otherwise noted. Detailed comments about the individual minerals and comparison with spectra of other authors are included in the tables and appendix. In the tables, vibrational bands are listed, with a vertical spacing approximately proportional to frequency or wave number, in a way that schematically shows the distribution of modes. For clarity and simplicity in the tables, modes reported by different authors are

TABLE 1. Vibrational Modes (**K** = 0) of Simple Substances

Halite		Periclase		Brucite		Corundum		Spinel	
w, cm^{-1}	Activity	w, cm^{-1}	Activity	w, cm^{-1}	Activity	w, cm^{-1}	Activity	w, cm^{-1}	Activity
				3688	IR				
				3652	R				
								825	*R* (weak, impurity?)
						751	R		
		730	INS	725	R			750–688	IR, R
						645	R	663	R
				633	INS	635	IR		
						583	IR	600	R
						578	R	580	IR
						569	IR	555	R
				461*	IR	451	R	522	IR
						442	IR	485	R
				443	R	432	R	463	R
				416	IR	418	R	435	R
		390	INS			400	IR	405	R
				361*	INS, IR	385	IR	375	R
						378	R	330	R
								309	IR
256	INS			280	INS, R			280	R
								225	R
173	INS								

Halite frequencies are from *Raunio et al.* [1969]. Periclase data are from *Sangster et al.* [1970]. Brucite INS data are from *Safford et al.* [1963], and IR data from *Buchanan et al.* [1963] and *Dawson et al.* [1973]. Corundum Raman data are from *White* [1975] and *Porto and Krishnan* [1967], and IR data from *Farmer* [1974*e*] and *Barker* [1963]. Spinel IR data are from *Preudhomme and Tarte* [1971*a*, *b*, *c*, 1972], and Raman data are from *Fraas and Moore* [1972] and *Fraas et al.* [1973].
*Value confirmed by this study.

considered to be the same mode if they lie within ±5 cm^{-1} of each other.

(The terminology used by spectroscopists and solid-state physicists to describe vibrational modes is inconsistent. On plots of dispersion curves, the wave vector **K** (in cm^{-1}) is given versus frequency ω (in radians per second) or ν (in cycles per second or terahertz). However, for optical spectra taken at **K** = 0 it is common to give these frequencies as wave numbers w (= $\omega/2\pi c$) in cm^{-1} or even as wavelength λ (in micrometers). The quantity w should be called a wave number rather than a frequency. The most common convention in optical spectroscopy is to specify w; however, in INS work, frequency is given as ν or ω. Hence some mixing of units is unavoidable if one attempts to use units common to the various experimental techniques.)

The mid-infrared and far-infrared data shown in Figure 1 were obtained with a Perkin Elmer 180 infrared spectrophotometer. For the mid-infrared study (1200 > w > 300 cm^{-1}), ~100 mg of powdered sample were mixed with 200 mg of KBr powder and pressed into disks to 20,000 psi (about 1.5 kbar) pressure under vacuum. Successive spectra obtained under the same operating conditions were reproducible to within ±2 cm^{-1}. For the far-infrared study (w < 400 cm^{-1}), small amounts of specimen powder were mixed with Vaseline petroleum jelly on polyethylene plates. Successive spectra were taken with varying amounts of powder to obtain maximum absorption in weak features. The scanning speed was variable, generally from 5 to 10 cm^{-1}/min, and the slit width was also variable. Mid-infrared and far-infrared spectra overlapped in the region 300–400 cm^{-1}. Lines in this region of overlap were reproducible to ±2 cm^{-1} with the two techniques. All spectra were taken at room temperature.

General features of optical spectra of minerals and the variations of these features within mineral composition and structure are well known and will not be reviewed here. Excellent reviews are given by *Lazarev* [1972], *Farmer* [1974*a*] and *Karr* [1975]. The reader should note the following major features and trends important to the thermodynamic properties considered here: (1) the very broad range of frequencies spanned by the optical modes, (2) the dependence of the highest-frequency modes on the degree of polymerization of the Si-O bond, and (3) the dependence of the frequency of the lowest modes on cation-oxygen bonds. These points are discussed in detail in section 4.

TABLE 2. Vibrational Modes (**K** = **0**) of Framework Silicates, Stishovite, and Rutile

Quartz		Cristobalite		Silica Glass		Coesite		Stishovite		Rutile		Albite (Low)		Microcline	
w, cm^{-1}	Activity	w, cm^{-1}	Activity	w, cm^{-1}	Activity	w, cm^{-1}	Activity	w, cm^{-1}	Activity	w, cm^{-1}	Activity	w, cm^{-1}	Activity	w, cm^{-1}	Activity
1230	R	1202	IR	1200	R	1229	IR					1150	IR	1142	IR
1160	R, IR	1160	IR	1184	IR	1155	IR					1096	IR, R	1134	IR
1082	R, IR	1095	IR	1098	IR	1100	IR					1032	IR, R	1120	IR
1064	R							(1085?)	IR			990	IR, R	1100	IR
1055	IR			1055	R	1040	IR					977	R	1044	IR
														1010	IR
						(960?)	IR	960	IR						
						(880?)	IR								
								880	IR	841	IR, INS				
						(840?)	IR			824	R, INS				
						(811?)	IR			810	IR	814	R		
800	R, IR	795	IR	804	IR, R	792	IR					784	IR		
780	R, IR							769	IR			762	R, IR	768	IR
								735	IR			740, 720	IR	742	IR
695	R, IR			695	IR	681	IR	670	IR			648	IR, R	728	IR
		623	IR					633	IR			604, 588	IR		
				605	R					610	R, INS	579	R	648	IR
						599	IR					528	IR, R	602	IR
		515	IR			561	IR	562	IR			506	R	584	IR
		490	IR	490	R	(490?)	IR			493	IR, INS	476	IR, R	535	IR
466	R, IR			468	IR	448	IR			444	R, INS	463	IR	463	IR
452	R			440	R	438	IR			428	IR, INS	453	R	428	IR
						420	IR			406	INS	425	IR		
397	R	383	IR			394	IR			388	IR	415, 406	R	398	IR
365	IR					375	IR			374	IR, INS	400, 388	IR	378*	IR
356	R					337	IR	330	IR			376, 336	IR	332*	IR
		298*	IR			296	IR					328, 297	IR		
264	R, INS					265	IR	285	IR			288, 266	R	(278*?)	see Figure 1*d*
207	R, INS							220(?)	IR			252, 249	IR	(186*?)	discussion
										189	IR, INS	221, 207	R	150*	IR
128	R, INS					140(?)	IR			172	IR, INS	200	IR	136*	IR
		100 ↓								141	R, INS	185*; 179	IR; R	115*	IR
				48? ↓						113	INS only	165*, 148*	IR	98*	IR
												92*	IR	74†	
												83*	IR		

Quartz Raman and IR data are from *Lord and Morrow* [1957] and *Scott and Porto* [1966], and INS data are from *Elcombe* [1967]. Cristobalite IR data for $w > 490$ cm^{-1} are from *Moenke* [1974] and for $w < 400$ cm^{-1} from this study; Raman data are not available. The arrow from $w = 298$ to $w = 100$ cm^{-1} indicates that an intense absorption continuum exists in this region as suggested by *Leadbetter* [1969]. Silica glass IR data are from *Lyon* [1962], and the Raman data are from *White* [1975] and *Flubacher et al.* [1959]. The intense Raman continuum for $w < 560$ cm^{-1} with intensity maxima at 48, 440, and 490 cm^{-1} [*Flubacher et al.*, 1959] is indicated by an arrow. Coesite IR data are from this study (Figure 1) and agree well with data of *Lyon* [1962]; Raman data are not available. Stishovite IR data are from this study (Figure 1) except for the 769-cm^{-1} band (reported by *Lyon* [1962]); Raman data are not available. Rutile data are from *Traylor et al.* [1971]. Albite IR data are from *Iiishi et al* [1971], and Raman data are from *White* [1974]. Microcline IR data are from *Iiishi et al.* [1971]; Raman data are not available.

*Value confirmed by this study.

†Value not found in this study but reported in referenced work.

TABLE 3. Vibrational Modes (**K** = 0) of Chain and Sheet Silicates

Jadeite		Diopside		Enstatite		Muscovite	
w, cm^{-1}	Activity	w, cm^{-1}	Activity	w, cm^{-1}	Activity	w, cm^{-1}	Activity
						3633	IR
		1070	IR			1062	IR
		1048	R	1045	IR	1022	IR
1065	IR	1010	R	1010	R		
995	IR	965	IR			990	IR
940	IR	920	IR	938	R	935	IR
		865	IR				
860	IR	854	R	863	R	833	IR
						803	IR
748	IR			758	R	754	IR
718	IR	710	R	715	R	727	IR
				681	R, IR	697	IR
		664	R, IR	650	R	669 (vw)	IR
668	IR	630	IR			620	IR
615	IR	610	R				
590	IR	557	R	545	R	553	IR
		523	R	523	R		
		510	IR	500	IR		
470	IR	507	R			479	IR
435	IR	470	IR	450	IR		
408	IR	465, 417	R			412	IR
395*	IR	395; 389	IR; R	397	R, IR		
368*	IR	366; 357	IR; R	375	R		
328*	IR	335*, 323	IR; R	350	IR	352	IR
(313, 288?)		310*	IR	340	R		
255*	IR	292*	IR	275	IR		
		245*	IR	234	R, IR	263	IR
176*	IR	220*	IR	~190	IR	192	IR
152*	IR	150*	IR			186	IR
(138*?)		140†	IR	~110	IR	143	IR
		75†	IR			110	IR

Jadeite data for $w > 400$ cm^{-1} are from *Moenke* [1962] and for $w < 400$ cm^{-1} from this study; Raman data are not available. Diopside IR data are from *Omori* [1971*a*], and Raman data from *White* [1975]. Enstatite mid-IR data are from *Liese* [1975], far-IR data from *Kovach* [1975], and Raman data from *White* [1975]. Muscovite data are from *Farmer* [1974*c*] and *Ishii* [1967]; vw signifies very weak.

*Value confirmed by this study.

†Value not found in this study.

Inelastic Neutron Scattering Data

Inelastic neutron scattering data provide information about the frequency of both acoustic and optic modes across the Brillouin zone from $\mathbf{0} \leq \mathbf{K} \leq \mathbf{K}_{max}$. INS data are available for five minerals: halite, periclase, rutile, calcite, and quartz (Figure 2). The reader should note several important features not available from optical data alone.

The behavior of acoustic modes. Acoustic modes have zero frequency at $\mathbf{K} = \mathbf{0}$ and therefore are not included in infrared and Raman data which are taken at $\mathbf{K} = \mathbf{0}$. INS data show the acoustic branches throughout the Brillouin zone and thus reveal the degree of anisotropy and dispersion in the branches.

The presence of modes not optically active. Some optic modes are inactive under both IR and Raman conditions, e.g., the lowest mode at 113 cm^{-1} in rutile. This mode is especially important in consideration of the thermodynamic properties because it contributes significantly to the low-temperature heat capacity.

The dispersion of optic modes across the Brillouin zone. The frequency of the optic modes changes as **K** increases from the zone center to the zone boundary. The frequency may either increase or decrease with increasing wave vector. The change may be slight, as it is for the highest-frequency optical modes of quartz, in which case the modes are well approximated by an Einstein oscillator, or the change may be large, as it is for the longitudinal optic branch of halite, in which case the mode is not well represented by an Einstein oscillator. The dispersion of the modes across the Brillouin zone is significant in terms of thermodynamic calculations because the modes near the Brillouin zone boundary ($\mathbf{K} = \mathbf{K}_{max}$) are more heavily weighted in the frequency spectrum than those at the zone center ($\mathbf{K} = \mathbf{0}$), as can be seen by examination of (4) in paper 1 [*Kieffer*, 1979*a*].

Complete Vibrational Spectra

The complete vibrational spectra represent integrations of the individual branches over the entire Brillouin zone. Complete vibrational spectra for halite, periclase, and rutile, calculated from INS data and lattice models, are shown in Figure 3. Because of the dispersion of optical modes and, to a certain extent, because IR or Raman (or even the combination of infrared plus Raman) data alone give an incomplete represen-

TABLE 4. Vibrational Modes (K = 0) of Orthosilicates

Olivine		Zircon		Kyanite		Andalusite		Sillimanite		Pyrope		Andradite		Grossular		Calcite	
w, cm^{-1}	Activity	w, cm^{-1}	Activity	w, cm^{-1}	Activity	w, cm^{-1}	Activity	w, cm^{-1}	Activity	w, cm^{-1}	Activity	w, cm^{-1}	Activity	w, cm^{-1}	Activity	w, cm^{-1}	Activity
								1195?	IR							1432	R, IR
								1175	IR								
				1162†	IR			1110	IR								
				1075†	IR											1097	R
		1008	R	1033	IR	1005?	IR										
993	IR	984	IR,R	998	IR	970	IR			995	IR			951	IR		
960	IR, R	974	R	940	IR	940	IR	955	IR	965	IR	929	IR	905	IR		
922	R	885	IR	895	IR	895	IR	910	IR	897	IR	888	IR	852	IR	879	IR
880	IR, R							882	IR	870	IR	831	IR	834	IR		
860	R											811	IR	750			
837; 828	IR; R			795†, 775†	IR	774	IR	815	IR								
				721	IR	737	IR										
								745	IR								
				670	IR	688	IR	690	IR							714	R, IR
				635	IR			630	IR								
				620	IR									617	IR		
613	IR, R	608	IR	603	IR	609	IR										
595, 588	R			584	IR			582	IR	580	IR	589	IR	540	IR		
546	R			564	IR	561	IR			536	IR	510	IR	502	IR		
507	IR			543	IR			540, 525	IR	492	IR	477	IR	476	IR		
475, 462	IR			505	IR	520	IR	505	IR	458	IR	438	IR	445	IR		
442; 421	R; IR	439	R	465	IR	480	IR	490	IR			400	IR				
415	R; IR	430	IR	435	IR	455, 445	IR	437	IR								
408	IR	393	R, IR	395	IR					386 (385*)	IR	383*	IR	385 (392*)	IR	398	INS
381	IR, R			382	IR	388	IR	372	IR	345 (335*)	IR	348*	IR	(350*)	IR	381	INS
361	IR	357	R	361, 351	IR	365	IR	343	IR			310*	IR	(297*)	IR	303	INS
337, 330	R	338	IR	340	IR			334	IR							284	R
319; 312	IR; R			326	IR			319	IR	248 (248*)	IR	(250*?)	IR	238 (246*)	IR	239	INS
305; 301	R; IR	287	IR	314	IR	302	IR			209 (199*)	IR	211 (214*)	IR	200 (205*)	IR	223	INS, IR
295; 276	IR	266	R	294	IR			262	IR			187 (187*)	IR	180 (185*)	IR	172, 156	INS, R
244, 231	R	225	R	275	IR					149 (133*)	IR	(152*)	IR	(158*)	IR	136, 123	INS
224, 201	IR	215, 201	R	237	IR	204	IR	202	IR			132 (132*)	IR			102	INS, IR
186; 144	R; IR					156	IR	115	IR							92	INS, IR

Olivine IR data are from *Oehler and Günthard* [1969], and Raman data are from *White* [1975]. Zircon data are from *Dawson et al.* [1971]. Kyanite, andalusite, and sillimanite data are from this study (Figures 1*b* and 1*c*); earlier work was by *Lazarev* [1972] and *Tarte* [1963]; Raman data are not available for Al_2SiO_5 polymorphs. Pyrope-71, andradite-93, and grossular-92 data are from *Moore et al.* [1971]; Raman data are not available. Calcite INS data are from *Cowley and Pant* [1973], and Raman and IR data are from *Cifrulak* [1970] and *White* [1974]; Raman data are from *Scheetz and White* [1977].

*Value confirmed by far-infrared observations of this study.

†Weak lines.

TABLE 5. Data on Minerals of Tables 1–4 and Figure 1

Mineral	Source	Catalog Number	Analysis
		Powder X Ray Diffraction	
Brucite	United States	UCLA MS 707	pure (<1% graphite)
Kyanite	Litchfield, Connecticut	UCLA MS 3425	pure
Andalusite	Brazil	Grieger M 821-4	pure
Sillimanite	Antarctica		pure
Albite	Catalina Island, California	UCLA MS 2394	nearly pure, trace (estimated to be < 1%) of impurity, with d = 2.95, 3.74 Å
Microcline	Crystal Peak, Colorado	UCLA MS 2378A (blue) UCLA MS 2378B (white)	nearly pure, trace of impurity, with d = 3.17, 3.70 Å
Jadeite	Clear Creek	UCLA MS 2970A	nearly pure, trace of feldspar possible
Diopside	Ontario, Canada	UCLA MS 2947	nearly pure, trace of calcite and/or feldspar possible
		Microprobe Analyses	
Pyrope	Garnet Ridge, Kayenta, Arizona	UCLA MS 3250	$(Mg_{2.16}Ca_{0.36}Fe_{0.46}Mn_{0.03})(Al_{1.83}Cr_{0.13}Fe_{0.03})Si_{3.02}O_{12}$
Grossular	Asbestos, Quebec, Canada	UCLA MS 3263	$(Ca_{2.84}Mn_{0.03}Fe_{0.11})(Al_{2.01})Si_{3.01}O_{12}$
Andradite	Stanley Butte, Arizona		$(Ca_{2.97}Mn_{0.02})(Fe_{1.97}Al_{0.04})Si_{2.99}O_{12}$

For microprobe analyses, control samples of wollastonite, magnetite, pyrope, and andradite were run. Errors were estimated to be less than ±2%. The sillimanite sample was courtesy of Ed Grew, University of California, Los Angeles, and the andradite samples were courtesy of G. Rossman, California Institute of Technology, and J. Rosenfeld, University of California, Los Angeles. Microcline (white) was used for X ray analysis.

tation of the spectra, the complete vibrational spectra are more complex, and the modes are generally more evenly distributed, than would be believed from inspection of a list of modes obtained from optical data alone. This conclusion will provide the basis for an extremely simple model of the optic mode distribution in paper 3.

4. Interpretation of Vibrational Spectra

It was demonstrated in paper 1 that acoustic modes and low-frequency and high-frequency optic modes contribute to the observed deviations of silicates from Debyelike behavior. From the data presented above, the following generalizations about these three spectral regions can be drawn.

Acoustic Modes

In general, there are three distinct acoustic modes in each direction in reciprocal space, two transverse modes and one longitudinal mode. In high-symmetry directions the two transverse branches may be degenerate. For individual minerals the acoustic velocities and hence the slopes of the acoustic branches may vary by a factor of approximately 2. All acoustic modes show dispersion as the Brillouin zone boundary is approached. Many of the modes show approximately the sinusoidal shape predicted by the simple one-dimensional monatomic model ((23) of paper 1), but a few modes do show strong deviation from the sinusoidal dispersion law.

Low-Frequency Optic Modes

For most minerals for which far-infrared data are available, Raman and INS data are not available at low wave numbers. Because of the selection rules (which prevent some modes from being active under infrared conditions), the infrared data taken alone must be considered to be incomplete. Even where both Raman and far-infrared data are available, there is more than the usual amount of discrepancy in spectra reported by different authors because of experimental difficulties in the low-frequency region (e.g., transparency of samples and presence of water vapor lines). Some of the discrepancies are discussed in the table and figure captions.

The presence of modes near and below 100 cm^{-1} and their importance to thermodynamic properties have not been widely recognized, and very few data exist below 300 cm^{-1} to provide a basis for generalizations about the far-infrared optic spectrum. As an illustration of the importance of these modes at low wave numbers, consider an example taken from paper 3: at 25°K, more than half of the heat capacity of microcline is due to low-frequency optic vibrations, and at higher temperatures (to ~100°K) the heat capacity behavior is dominated by the vibrations near 100 cm^{-1}. In most minerals the low-frequency optic modes have a similar relative importance.

High-Frequency Optic Modes

The highest-energy optic modes observed in the anhydrous silicate minerals are in the region 900–1200 cm^{-1}, at wave numbers which are much larger than values obtained for acoustic Debye frequencies for silicates. For example, a Debye temperature of $\theta_{el} \sim 500$°K would correspond, if interpreted in terms of (10) of paper 1, to a characteristic maximum lattice frequency of $\sim 6.5 \times 10^{13}$ s^{-1}. For photons interacting with phonons of such frequencies the corresponding wave numbers would be ~350 cm^{-1}. It is thus evident that the actual vibrational spectra contain, in addition to the necessary acoustic portion at low frequencies, an array of vibrations extending to much higher frequencies than the upper limit that would be anticipated from the form of a Debye spectrum.

This state of affairs can be expected from the structural features of silicates. The strong Si-O bond, with a high force constant, binds local portions of the structure together into tight units, whose more or less localized internal stretching vibrations contribute high frequencies to the vibrational spec-

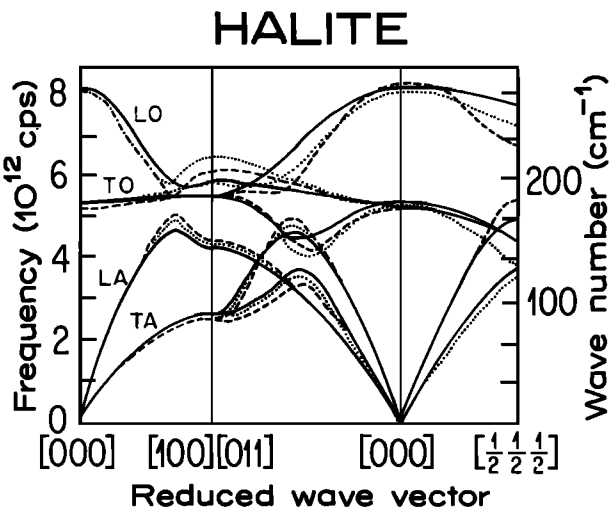

Fig. 2*a*. INS spectra of halite [*Raunio et al.*, 1969] clearly showing the dependence of the mode energy on the magnitude and direction of the wave vector **K**. Solid, dashed, and dotted lines represent a shell model, a deformed dipole model, and a breathing shell model, respectively; experimental data are in generally close agreement. Transverse optic (TO) modes are relatively flat (e.g., for the [100] direction the TO branch varies from $\sim 5.1 \times 10^{12}$ cps (~ 170 cm^{-1}) at $\mathbf{K} = 0$ to $\sim 5.2 \times 10^{12}$ cps (~ 173 cm^{-1}) at the zone boundary and reaches an intermediate maximum of $\sim 6.0 \times 10^{12}$ cps (202 cm^{-1}) at 0.8 $\mathbf{K}_{max}$). Longitudinal optic modes show much larger dispersion (e.g., for the [100] direction the LO branch varies from $\sim 7.5 \times 10^{12}$ cps (~ 256 cm^{-1}) at the zone center to $\sim 5.7 \times 10^{12}$ cps (~ 192 cm^{-1}) at the zone boundary). At the zone boundary the transverse and longitudinal optic branches are separated from the corresponding transverse and longitudinal acoustic branches, in qualitative agreement with the stopping band predicted from the diatomic chain model. The frequency ratios TO/TA and LO/LA at the zone boundary are 2.07 and 1.36, respectively, larger than would be predicted by a simple chain model dependence on the square root of the mass ratio, $(35/23)^{1/2} = 1.23$.

trum. During broad-scale compression or deformation of the structure, as occurs in the propagation of low-frequency acoustic waves, the tightly bound units tend not to compress or deform internally but instead to shift in relation to one another by the distortion of weaker bonds, with lower force constants, between the tightly bound units. In orthosilicates the relatively weak bonds are the cation-oxygen bonds such as Mg-O. In tectosilicates, bending of the Si-O-Si linkages provides the soft mechanism for relative shifts of SiO_4^{-4} tetrahedra. In silicates of intermediate polymerization, both mechanisms operate. The soft deformation mechanisms dominate the elastic behavior so that the acoustic velocities are relatively low, a (in (6) of paper 1) is large, and the inferred cutoff frequency ω_D (from (9) of paper 1) is relatively small. The hard deformation mechanisms dominate the high frequencies in the actual spectrum. The frequencies of vibration of the tightly bound units are thus shifted to frequencies higher than would occur in the absence of any change of effective force constant with frequency and hence are higher than the inferred ω_D.

In order to interpret vibrational modes of complex crystals and to distinguish between vibrations arising from hard and soft deformations, spectroscopists and molecular physicists frequently attempt to identify a priori the well-bound molecules and polyatomic clusters (such as ionic radicals) within crystals [*Herzberg*, 1945; *Venkataraman and Sahni*, 1970]. The concept of identification of clusters was developed in the treatment of isolated molecules, but since many solid-state problems are greatly simplified by the identification of clusters, it is advantageous to extend this concept as far as possible into considerations of solid substances. In this paper a 'molecule' of a substance will be taken as the group of atoms on which the chemical formula is based, and a 'molecular group' or 'cluster' as more tightly bound members of the molecule, for example, isolated SiO_4^{-4} tetrahedra, AlO_4^{-5} tetrahedra, CO_3^{-2} clusters, or structural chains, rings, or octahedra. If the groups are treated as rigid bodies (with due consideration for the coupling between various cluster units in the crystal), translational and rotational modes of the rigid bodies can be enumerated. These modes, plus translational modes of the individual ions, are the so-called 'external modes' of vibration. Effects due to nonrigidity of the molecular groups may be examined separately; these are the so-called 'internal modes.' It is useful to consider further the bond stretching and bond bending of the molecular groups separately. This concept was introduced by *Mecke* [1930*a*, *b*], and is also found in the work of *Herzberg* [1945], who postulated that to every bond in an isolated group there corresponds a high-frequency vibration in which it is stretched and a lower-frequency vibration in which it is bent. Although this concept was developed for isolated molecules, it will be demonstrated that it is useful to examine minerals in a similar way.

Molecular clusters can be treated as rigid bodies if the forces coupling atoms within the group are much stronger than those coupling the clusters together in the crystal [*Venkataraman and Sahni*, 1970, p. 411]. Experimental evidence which may be used to indicate clustering is two-fold.

1. A close similarity of the vibrational frequencies of the isolated group (e.g., in a vapor) and of the groups in the crystal is an indication that bonding within a cluster is strong in

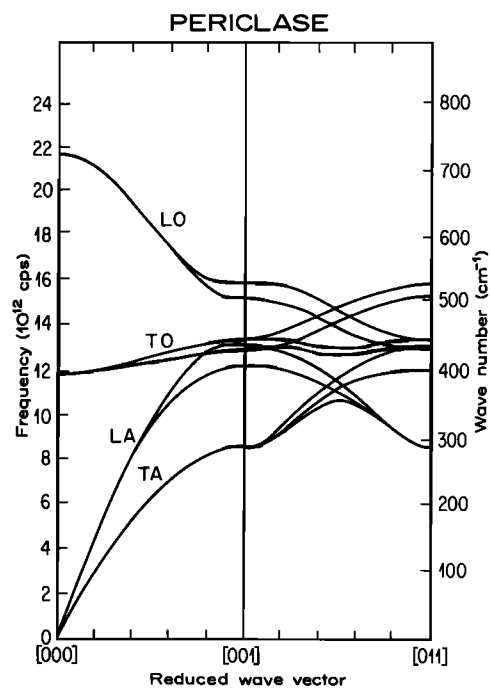

Fig. 2*b*. INS spectra of periclase [*Sangster et al.*, 1970] showing that the TO mode is relatively flat and that the LO mode is more strongly dispersed (e.g., for the [001] direction the TO mode varies from $\sim 11.7 \times 10^{12}$ cps (~ 390 cm^{-1}) at $\mathbf{K} = 0$ to about $\sim 12.9 \times 10^{12}$ cps (~ 430 cm^{-1}) at the zone boundary; the LO mode varies from $\sim 21.9 \times 10^{12}$ cps (~ 730 cm^{-1}) at the zone center to $\sim 15.9 \times 10^{12}$ cps (~ 530 cm^{-1}) at the zone boundary). The acoustic branches are nearly sinusoidal in form in the high-symmetry directions ([100] and [111]) in which the TA branch is degenerate, but they are much more irregular in shape in the other directions. The curves shown are for a breathing shell model; they agree well with experimental data which are not reproduced in the figure.

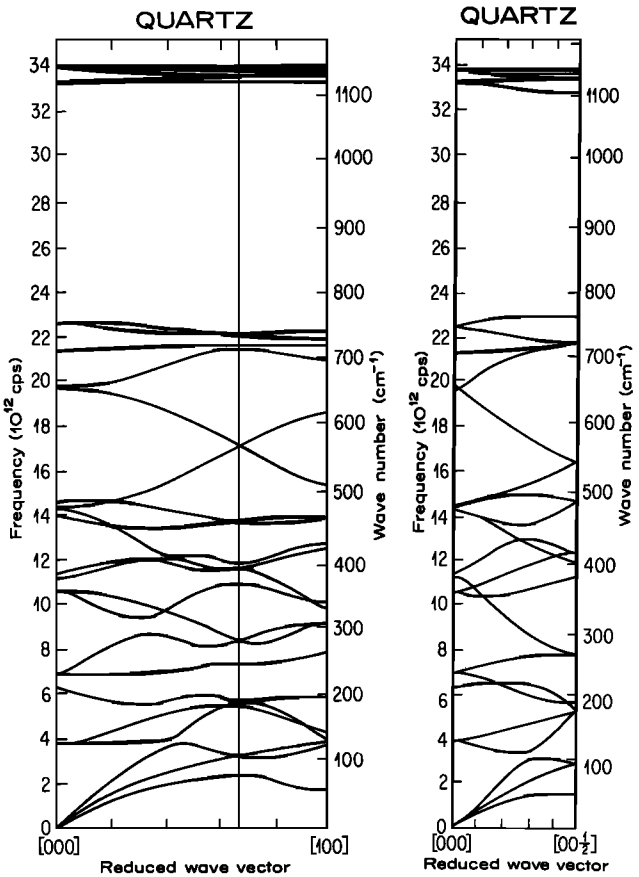

Fig. 2c. Dispersion curves of α-quartz [*Elcombe*, 1967] calculated from a Born–von Karman model. The seven lowest curves with wave vectors in the z direction were also measured by INS at room temperature. The calculated curves are in good qualitative agreement with the measured data but agree quantitatively for only a few branches. All six modes in the upper band correspond to atomic vibrations in which the length of the silicon-oxygen bond changes.

relation to bonding between clusters. Characteristic group frequencies are observed in different molecules containing the same groups [*Herzberg*, 1945; *Moenke*, 1974, p. 11]. For example, all molecules containing the triple C≡H bond are observed to have vibrational modes at about 3300 and 700 cm^{-1} (e.g., C_2H_2 and HCN). The values of the wave numbers of these modes usually hold within ±100 cm^{-1} in the different molecules. Another example is found in the silicates: all molecules containing tetrahedrally coordinated silicon are observed to have a complex absorption band due to Si-O stretching in the range 800–1100 cm^{-1}, independent of the construction of the silicon-oxygen radical as reported by *Saksena* [1961] and many others. The exact position of this band is affected by the degree of polymerization of the SiO_4^{-4} tetrahedra, being at highest energies (~1100 cm^{-1}) in framework silicates, at ~1000 cm^{-1} in the chain silicates, and at the lowest frequencies (~900–950 cm^{-1}) in orthosilicates (see the studies by, for example, *Griffith* [1969*a*, *b*], *Keller et al.* [1952], *Launer* [1952], *Hunt et al.* [1950], and *White* [1975]). Aluminum oxides and aluminum-containing silicates have characteristic vibrational frequencies associated with Al-O stretching modes. If aluminum is in fourfold covalent coordination with oxygen (e.g., in albite, orthoclase, and leucite), a characteristic vibration band is observed in the region 720–780 cm^{-1} [*Kolesova*, 1959]. In these compounds, the Al-O distances are 1.72–1.75 Å. If, however, the aluminum atoms do not enter the 'anion shell' of the silicate but replace alkali and alkaline-earth metals, not silicon atoms, then the coordination number of aluminum atoms is six, the bond is mainly ionic, and the Al-O distance is 2.1 Å. In this case the complex band at 720–780 cm^{-1} is missing. The Al-O stretching modes occur in a range of wave numbers common to many other cation-oxygen modes, e.g., the Si-O bending modes, and it is therefore not always possible to identify and enumerate the Al-O stretching modes in mineral spectra.

2. A large difference in force constants within a crystal indicates clustering. Relative values of the bond-stretching and bond-bending force constants, which have been calculated for isolated or linked SiO_4^{-4} tetrahedra by various authors [*Saksena*, 1942, 1945; *Lazarev*, 1972; *Elcombe*, 1967], provide a semiquantitative basis for separating soft and hard deformations. For example, on the basis of a Born–von Karman model, *Elcombe* [1967] assigned a value of 4.33 × 10^5 dyn to the silicon-oxygen stretching force constant and a much smaller value of 0.54 × 10^5 dyn to the O-Si-O bond bending force constant for isolated SiO_4^{-4} tetrahedra. Although other linkages in crystals may alter the values of these force constants somewhat, the relatively high strength of the stretching force constant compared to the bending force constant appears to be retained in most structures in which the tetrahedra are identifiable units.

Semiquantitative assignment of observed modes to 'external' and 'internal' modes of the clusters is relatively easy for crystals in which the clusters are isolated units, e.g., NH_4Cl, $NaNO_2$ [*Venkataraman and Sahni*, 1970], and, of the cases of interest here, orthosilicates. However, the problem of internal mode enumeration is more complicated in polymerized lattices than in molecular lattices because the quasi-molecular units which act as molecular clusters with respect to stretching vibrations are, in fact, linked together in various ways such that a unit cell or formula unit does not represent or contain within it integral units of the isolated molecular cluster; for example,

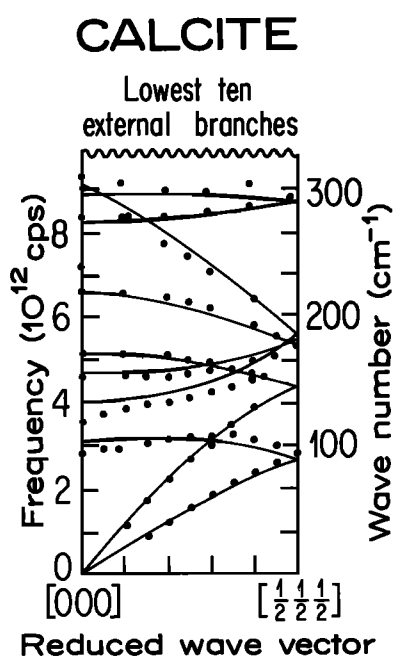

Fig. 2d. INS spectra of calcite for the ten lowest branches [*Cowley and Pant*, 1973]. There are a total of 30 branches: 12 correspond to internal motions of the carbonate groups and have frequencies between 21 and 43 × 10^{12} cps (700 and 1440 cm^{-1}); the remaining 18 are external vibrations and have frequencies ranging up to 12 × 10^{12} cps (400 cm^{-1}). The curves are calculated with a shell model which contains 10 adjustable parameters.

in quartz the cluster is not an SiO_2 molecule but is the SiO_4^{-4} tetrahedron. Thus some scheme must be devised which accounts correctly for the sharing of oxygens among the quasi-molecular clusters.

Consider first the silicates in which silicon is in tetrahedral coordination. Each silicon is surrounded by four oxygens, giving five particles per cluster. Therefore an isolated tetrahedron would have 15 degrees of freedom. Of these, (5 − 1 =) 4 would be stretching modes; in a simple way, one can think of one stretching mode per independent Si-O bond. If the tetrahedra are linked to form a simple chain, two oxygens per silicon are shared, and one oxygen per silicon is removed from the formula (as is implied in the pyroxene formula $XSiO_3$). In this case there are only four particles per cluster ($Si + O_{nonbr} + O_{nonbr} + \frac{1}{2}O_{br} + \frac{1}{2}O_{br}$, where nonbr stands for a nonbridging oxygen and br for a bridging oxygen), and there are only 12 degrees of freedom per cluster, of which (4 − 1 =) 3 are stretching; in a simple way, this implies one stretching mode for each Si-O bond with a nonbridging oxygen and a shared mode for the silicon between the bridging oxygens. Similarly, in a framework silicate, in which all oxygens are shared, two oxygens per silicon are removed, as is implied in the formula SiO_2 or $X(Si, Al)_4O_8$. In this case, there are only three particles per cluster ($Si + \frac{1}{2}O_{br} + \frac{1}{2}O_{br} + \frac{1}{2}O_{br} + \frac{1}{2}O_{br}$) and hence only 9 degrees of freedom per cluster, of which (3 − 1 =) 2 are internal stretching modes. Amphiboles and sheet silicates represent intermediate cases between the single chains and the framework silicates and can be treated similarly.

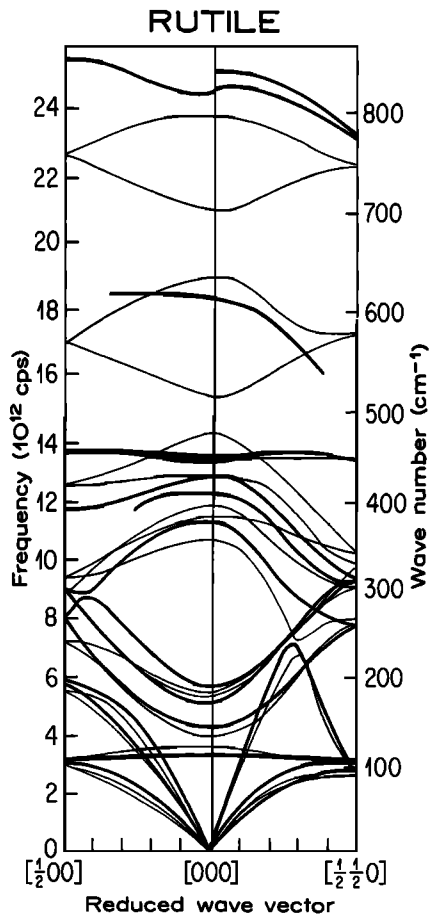

Fig. 2e. Dispersion curves of rutile at room temperature: measured curves (heavy) and shell model curves (light) from *Traylor et al.* [1971]. INS data show that the frequency of the low-frequency optic mode at 5.18 × 10^{12} cps (172 cm^{-1}) at **K** = 0 decreases by 18% to 4.25 × 10^{12} cps (142 cm^{-1}) at 4.2°K.

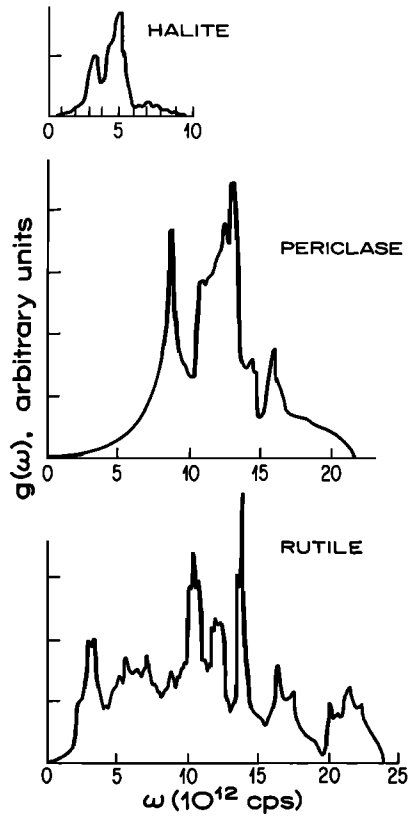

Fig. 3. Vibrational spectra of halite, periclase, and rutile. For halite [*Neuberger and Hatcher*, 1961] the frequency distribution function was calculated from an extended form of the Born and Blackman anharmonic potential theory applied to the Kellerman model of the NaCl crystal. For periclase [*Sangster et al.*, 1970] the frequency distribution was obtained from the breathing shell model shown in Figure 2. This spectrum gives a low-temperature heat capacity in good agreement with measured heat capacities. For rutile [*Traylor et al.*, 1971] the frequency distribution was obtained from the room temperature shell model shown in Figure 2. The distribution cannot predict the low-temperature heat capacity accurately because the frequency of the low-frequency optic mode at 5.1 × 10^{12} cps (172 cm^{-1}) changes with temperature.

Two substances with cations in octahedral coordination were examined in this study, stishovite and rutile. In this case, all cation-oxygen bonds are shared, e.g., each oxygen with three cations. Each cluster contains, conceptually, only three particles (e.g., $Si + \frac{1}{3}O + \frac{1}{3}O + \cdots$) and therefore has associated with it (3 × 3 =) 9 degrees of freedom, of which (3 − 1 =) 2 are stretching modes.

This enumeration scheme can be tested from spectral data for four minerals: quartz, calcite, zircon, and rutile. Consider first the internal stretching modes of quartz. For the unit cell of nine atoms the above scheme predicts six internal stretching modes per unit cell; these modes account for 22% of the total degrees of freedom. Neutron scattering data of *Elcombe* [1967, p. 954], shown here in Figure 2c, clearly show these six modes in an isolated narrow band between 1055 and 1172 cm^{-1}, separated by a wide gap from the next band at 767 cm^{-1}. The strongest feature in the (infrared) spectrum at 1055–1060 cm^{-1} was assigned as the main valence stretching ($\overleftarrow{Si}$-$\vec{O}$-$\overrightarrow{Si}$) vibration by *Simon and McMahon* [1953]. Assignments to other vibrations of the stretching modes have been given by *Saksena* [1940, 1961] and *Matossi* [1949].

For the calcite unit cell of 10 atoms the CO_3^{2-} ion is taken as the molecular cluster, and the above scheme predicts six stretching modes. Only five of the six stretching modes are active in infrared and Raman spectra (doubly degenerate

TABLE 6. Mode Partitioning for the Minerals

Mineral	Formula	n	$3n$	Cation X	Number of X-O Stretching Vibrations per X	q
Halite	NaCl	2	6			0
Periclase	MgO	2	6			0
Brucite	$Mg(OH)_2$	5	15	O-H	1	0.13
α-Corundum	Al_2O_3	5	15			0
Spinel	Al_2MgO_4	7	21	Mg	4	0.19
α-Quartz	SiO_2	3	9	Si	2	0.22
α-Cristobalite	SiO_2	3	9	Si	2	0.22
Coesite	SiO_2	3	9	Si	2	0.22
Glass	SiO_2	3	9	Si	2	0.22
Stishovite	SiO_2	3	9	Si	2	0.22
Rutile	TiO_2	3	9	Ti	2	0.22
Albite	$Na(Al_{1/4}Si_{3/4}O_2)_4$	13	39	(Si, Al)	2	0.205
Microcline	$K(Al_{1/4}Si_{3/4}O_2)_4$	13	39	(Si, Al)	2	0.205
Muscovite	$KAl_2(AlSi_3O_{10})(OH)_2$	21	63	(Si, Al)	2.5	0.159
				(O-H)	1	0.032
Talc	$Mg_3(Si_4O_{10})(OH)_2$	21	63	Si	2.5	0.159
				O-H	1	0.32
Enstatite	$MgSiO_3$	5	15	Si	3	0.20
Jadeite	$NaAl(SiO_3)_2$	10	30	Si	3	0.20
Diopside	$CaMg(SiO_3)_2$	10	30	Si	3	0.20
Tremolite	$Ca_2Mg_5Si_8O_{22}(OH)_2$	41	123	Si	2.75	0.179
				O-H	1	0.016
Forsterite	Mg_2SiO_4	7	21	Si	4	0.19
Zircon	$ZrSiO_4$	6	18	Si	4	0.22
Sillimanite	$Al^{VI}Al^{IV}O(SiO_4)$	8	24	Si	1	0.04
Kyanite	$Al_2{}^{VI}O(SiO)_4$	8	24	Si	4	0.167
Andalusite	$Al^{VI}Al^{V}O(SiO_4)$	8	24	Si	4	0.167
Pyrope	$Mg_3Al_2(SiO_4)_3$	20	60	Si	4	0.20
Grossular	$Ca_3Al_2(SiO_4)_3$	20	60	Si	4	0.20
Spessartine	$Mn_3Al_2Si_3O_{12}$	20	60	Si	4	0.20
Almandine	$Fe_3Al_2Si_3O_{12}$	20	60	Si	4	0.20
Andradite	$Ca_3Fe_2(SiO_4)_3$	20	60	Si	4	0.20
Calcite	$CaCO_3$	5	15	C	3	0.20

In this table, n is the number of particles per formula unit, X is the cation at the center of the group or cluster for which the stretching modes are being calculated, and q is the fraction of the total modes which are stretching modes.

modes at 1432 cm^{-1} (ν_3^g) and 1407 cm^{-1} (ν_3^u) and a single mode at 1088 cm^{-1} (ν_1^g)); the sixth mode (ν_1^u) is inactive but presumably lies at a frequency near 1088 cm^{-1} because the frequency splitting of antiphase and in-phase pairs ('factor group splitting') is only 25 cm^{-1} for the ν_3 mode, a mode which is similar in stretching deformation. Frequencies and displacements of atoms in the vibrations are given by *White* [1974, pp. 231–233]. The stretching modes are well isolated from the internal bending modes, the highest of which are at 872 and 712–714 cm^{-1}. Thus the above enumeration scheme works well for calcite.

The primitive unit cell of zircon contains 12 atoms. This model predicts eight stretching modes for the unit cell, i.e., four per tetrahedron. *Dawson et al.* [1971] find these modes at 974 cm^{-1} (ν_1) and at 1008, 989, and 885 cm^{-1} (ν_3). Therefore the model gives results in good agreement with the spectroscopic data.

An examination of data for rutile provides an opportunity to test the idea of quasi-molecular units and the above enumeration scheme for continuous frameworks of linked octahedra, for which we a priori might expect that the assumption of molecular clusters is weak. Many investigators have, in the past, found it convenient to adopt the idea of quasi-molecular units for purposes of interpreting the rutile spectrum, but the idea has not been universally accepted [e.g., *Matossi,* 1951; *Pandey,* 1965; *Porto et al.* 1967]. The above scheme gives four internal stretching modes per unit cell for the rutile unit cell of six atoms. Three of these modes, at 824, 841, and 810 cm^{-1}, are readily identifiable in neutron scattering experiments and related theory (see Figure 2*e*) and are assigned as predominantly stretching deformations by *Traylor et al.* [1971]. The fourth mode is either an A_{2g} (Mulliken notation) mode that has not been found in either optic or neutron work or an A_{1g} mode at 610 cm^{-1}. The mode which has not been found is a 'rocking mode' and seems to be an implausible candidate for an internal stretching mode; the 610-cm^{-1} mode is a stretching deformation. The four modes at 610, 824, 841, and 810 cm^{-1} are reasonably isolated from the bending modes which all lie at wave numbers below 500 cm^{-1}. Thus the assumption of quasi-molecular clusters and the above enumeration scheme can be extended with some qualification to rutile.

The success of the enumeration scheme in predicting the fraction of modes which are internal stretching vibrations for these four minerals suggests that it may be generally useful as a method of prediction for other minerals, for example, for chain and orthosilicates in which the silica tetrahedra are more polymerized and the Si-O linkages are nonlinear. Mode partitioning values, denoted by q, for all of the minerals considered in this study are given in Table 6.

5. Conclusions

General features of silicate vibrational spectra can be inferred from existing data, but for most minerals, data are insufficient to allow a detailed formulation of vibrational

properties. In general, it can be inferred that there are three acoustic branches which may show considerable anisotropy and dispersion; a sine wave dispersion law approximates the behavior of these branches in a qualitative way. Optic modes span a much wider range of frequencies than would be expected by application of a Debye model. The lowest optic modes are associated with cation-oxygen bending vibrations. They generally lie above the lowest transverse acoustic mode but may overlap the higher transverse acoustic and longitudinal acoustic modes. In some cases the optic modes occur as low as 75–100 cm^{-1}; in many cases, spectral data are not complete and the lowest-energy mode cannot be specified. Many of the higher-frequency optic modes are associated with Si-O or, in some cases, Al-O stretching vibrations and can be identified at characteristic frequencies. If molecular 'clusters' can be identified in the crystal, the fraction of total modes associated with internal stretching of the clusters can be calculated. Other than the acoustic modes and cluster stretching modes the optic modes do not appear to follow a simple recognizable distribution, such as a Debye distribution, but are rather widely dispersed across a range of frequencies.

APPENDIX

Notes for Table 1

Halite and periclase. Because of the highly ionic character of these compounds the single triply degenerate infrared-active mode predicted by simple theory is replaced by a broad band of absorption which corresponds rather closely to the restrahlen curve extending continuously from the lower-frequency transverse optic mode to the higher-frequency longitudinal mode [*Farmer, 1974b, e*]. There are no first-order Raman modes. Dispersion of modes is shown in Figure 2.

Brucite. The two modes at 3688 and 3652 cm^{-1} are associated with out-of-phase and in-phase stretchings of the hydroxyl group, respectively [*Buchanan et al., 1963, p. 1149*]. The remaining optically active modes [*Dawson et al., 1973*] are at lower energies than the MgO modes. A single broad acoustic mode has been observed in INS work at 120–135 cm^{-1} [*Safford et al., 1963*].

Corundum. Although complete Raman and infrared data are available for Al_2O_3, no satisfactory assignments have yet been published for the vibrations of the corundum structures [*Farmer, 1974e*]. There are six IR-active, seven Raman-active, and two inactive modes.

Spinel. Infrared spectra are available for spinels of varying compositions [*Preudhomme and Tarte, 1971a, b, c, 1972*], but Raman data are available only for a few spinels with Cr or V impurities. The IR spectra show four major features. In $MgAl_2O_4$ these features and their assignments are as follows: 680–750 cm^{-1}, Mg-O-Al stretching; 580 cm^{-1}, Al-O-Al stretching; 522 cm^{-1}, Al vibrating in opposition to Al; 309 cm^{-1}, Mg versus Al. Five Raman modes are predicted by theory [*White and De Angelis, 1967*], but ten are observed, possibly because of impurity resonant Raman effects [*Fraas and Moore, 1972; Fraas et al., 1973*].

Notes for Table 2

Quartz. Data may be considered to be complete and reliable. The highest frequency modes are associated with Si-O stretching modes.

Cristobalite. The high-frequency mode distribution is similar to that of quartz. The lowest infrared mode of cristobalite is at 298 cm^{-1}, much higher than the lowest vibrational mode of quartz. Raman data are not available, but INS data [*Leadbetter, 1969, p. 785*] show coherence effects as low as 100 cm^{-1}, and Leadbetter attributes these effects to optic modes; it should therefore be assumed that optic modes extend lower than the lowest mode revealed by infrared data.

Silica glass. The high-frequency mode distribution of glass is similar to that of quartz and cristobalite. The lowest optically active mode is a Raman-active mode at 440 cm^{-1}. However, the Raman spectrum shows an intense continuum extending from 560 cm^{-1} to 8 cm^{-1} [*Flubacher et al., 1959, p. 57*]. Within this continuum are intense bands at 48, 432, and 490 cm^{-1}, as well as the infrared band at 468 cm^{-1}. The cause of the continuum, its similarity to the cristobalite spectrum at wave numbers above 100 cm^{-1}, and its relation to the well-known excess heat capacity of vitreous silica have been the subject of much controversy [*Flubacher et al., 1959; Anderson, 1959; Clark and Strakna, 1962; Leadbetter, 1968*]. This controversy will be examined in further detail in paper 3.

Coesite. The high-frequency mode distribution of coesite is similar to that of quartz, cristobalite, and glass. It is reasonable to assume that the modes at $w > 1000$ cm^{-1} are Si-O stretching modes. The spectrum exhibits strong infrared absorption bands down to 265 cm^{-1}. A weak band is observed at 140 cm^{-1}; however, it cannot be assigned unambiguously to coesite. The sample of coesite on which the spectrum was taken was naturally shocked coesite recovered by HF acid treatment from shocked Coconino sandstone from Meteor Crater, Arizona [*Kieffer, 1971*]. This material was used because it is the same source material as was used in C_V experiments [*Holm et al., 1967*] and because pure synthetic coesite and stishovite are difficult to obtain. It contains traces of rutile and stishovite which may contribute weak lines to the infrared spectrum (Figure 1), stishovite lines at 960 and 880 cm^{-1} and possibly rutile lines at 490 and 140 cm^{-1}. Hence the weak lines in the coesite spectrum cannot be attributed with assurance to coesite, although the possibility exists that they are weak IR lines or even forbidden Raman lines appearing because a large amount of sample was used.

Stishovite and rutile. Stishovite and rutile are structurally similar and, in a simple model, might be expected to show vibrational differences arising solely from differences in cation properties, e.g., from mass differences. However, particularly high dipole moments are developed during vibrations involving displacement of Ti relative to O in rutile, and as a result the rutile spectrum is complex. The spectrum of stishovite is qualitatively similar to that of rutile: both have an absorption feature of considerable width isolated at high frequencies (830–1000 cm^{-1} for stishovite and 800–900 cm^{-1} for rutile), a second deep feature (800–600 cm^{-1} for stishovite and 500–370 cm^{-1} for rutile), and isolated lines at lower frequencies. Spectral features which may correspond (e.g., the highest bands in both spectra probably represent cation-oxygen stretching modes) are at higher wave numbers in the stishovite spectrum than in the rutile spectrum, as would be expected from the relative masses of the cations. The lowest observed infrared mode of stishovite is at 220 cm^{-1}; Raman data are not available. For comparison the lowest infrared-active mode of rutile is at 172 cm^{-1}, but there are two modes at even lower energies which are not IR active, a Raman mode at 141 cm^{-1} and an optically inactive mode which appears only in INS data at 113 cm^{-1}. The stishovite sample used was recovered from shocked Coconino sandstone from Meteor Crater, Arizona, and, as a result, was very fine grained ($d < 1000$ Å) and probably contained impurities of minerals not soluble in HF or HNO_3.

Albite and microcline. The spectra of albite and microcline show the lowest far-infrared bands of any minerals in this study, 92 cm^{-1} for albite and 98 cm^{-1} for microcline. Lower-energy bands in feldspars have been reported [*Iiishi et al.*, 1971; *Kovach et al.*, 1975] but were not confirmed in this study. The 98-cm^{-1} band was found in two different samples of microcline, but the 74-cm^{-1} line was not found, although a careful search of this spectral region was made.

The faint band at 83 cm^{-1} for albite (Figure 1*d*) has been found in Raman spectra of the same albite crystal (J. Delany, private communication, 1978).

Notes for Table 3

Jadeite and diopside. Relatively little spectral work has been done on jadeite, but a vibrational mode analysis of the IR absorption spectrum of diopside has been given by *Omori* [1971*a*] with the following results: modes at $w > 865$ cm^{-1} are Si-O stretching modes; the 630-cm^{-1} mode is a bending of nonbridging oxygen-silicon bonds; modes between 400 and 500 cm^{-1} are bending deformations of the chains; modes between 335 and 245 cm^{-1} are wagging, rocking, or bending of Si-O bonds; and the lower modes are chain-stretching modes. The lowest mode at 75 cm^{-1} reported by Omori was not found in a careful search in this study. Raman data do not extend into the low-energy region.

Enstatite. The high-frequency part of the enstatite spectrum is generally similar to that of diopside. The far-infrared bands near 400 and 350 cm^{-1} are sensitive to iron content and can be used to distinguish individual members in the enstatite-orthoferrosilite series [*Kovach*, 1975].

Muscovite. The band at 3633 cm^{-1} is an O-H stretching band. The bands in the region of 1000 cm^{-1} are Si-O stretching modes, the perpendicular Si-O vibration at 1062 cm^{-1} and the in-plane Si-O-Si stretching vibrations in the range 990–1062 cm^{-1} [*Farmer*, 1974*c*, p. 350]. Si-O bending vibrations contribute to strong absorption in the range 400–550 cm^{-1}; vibrations of the octahedral cations appear below 600 cm^{-1}. The band at 833 cm^{-1} is attributed to an Al-O out-of-plane vibration, and the band at 754 cm^{-1} to an Al-O-Si in-plane vibration. *Farmer* [1974*c*, p. 351] attributes the lowest-frequency band at 110 cm^{-1} to in-plane vibrations of the K^+ ion.

Notes for Table 4

Olivine. The two infrared-active modes of olivine observed at 993 and 960 cm^{-1} have predominately Si-O stretching character [*Oehler and Günthard*, 1969, p. 4726]. The modes near 613 cm^{-1} involve motions of the whole MgO_6^{-10} octahedron. Below 500 cm^{-1}, olivines which contain different divalent cations (M in M_2SiO_4, where M is Mg^{2+}, Fe^{2+}, Mn^{2+}, or Ca^{2+}) exhibit a fairly uniform infrared spectrum in which individual bands are sensitive to cation composition [*Kovach et al.*, 1975, p. 235]. Bands at 421, 408, 381, 361, 319, 295, and 276 cm^{-1} are assigned to strongly mixed modes of the whole set of atoms in the unit cell. The lowest bands at 224, 201, and 144 cm^{-1} have been attributed to mixed vibrational modes involving both the SiO_4 and MO_6 coordination polyhedra [*Oehler and Günthard*, 1969]. The lowest band at 144 cm^{-1} in Mg_2SiO_4 moves to progressively lower wave numbers as iron is added in solid solution; it is at 110 cm^{-1} in $(Fe_{80}Mg_{20})_2SiO_4$.

Zircon. Modes above 880 cm^{-1} are internal symmetric and antisymmetric stretching modes of the SiO_4^{-4} tetrahedra. Internal bending modes span the spectrum from 608 to 266 cm^{-1}; the 608-cm^{-1} mode is somewhat isolated from the next lower bending mode at 439 cm^{-1}. The external rotary and translational modes lie in a relatively narrow range between 400 and 200 cm^{-1} (mode assignments by *Dawson et al.* [1971]).

Kyanite, andalusite, and sillimanite. Spectra of kyanite $Al_2^{VI}(SiO_4)O$, andalusite $Al^{VI}Al^{V}(SiO_4)O$, and sillimanite $Al^{VI}Al^{IV}(SiO_4)O$ show the influence of the aluminum coordination number on vibrational features [*Lazarev*, 1972, p. 170]. Kyanite is a typical orthosilicate and shows three bands in the range 1040–940 cm^{-1} corresponding to the three components of the ν_{as} SiO_4^{-4} vibration and a weaker ν_s SiO_4^{-4} vibration at 895 cm^{-1}. The features at 1162 and 1075 cm^{-1} in Figure 1*b* are not visible in Lazarev's spectra. Lazarev attributes the numerous bands between 600 and 715 cm^{-1} to Al-O vibrations. Andalusite also shows characteristics of an orthosilicate in the high wave number region: it has three asymmetric stretching bands in the region 1005–940 cm^{-1} and the asymmetric stretching band at 895 cm^{-1}. Lazarev attributes bands in the region 600–700 cm^{-1} to Al-O vibrations. The Al-O bands probably occur at higher frequencies in andalusite than in kyanite because the covalency of the aluminum bonds with oxygen increases in fivefold coordination. In sillimanite, half of the aluminum atoms are in fourfold coordination and are ordered into $(Si_2Al_2O_{10})_\infty$ 'ribbons.' *Lazarev* [1972, p. 172] calculates that such a ribbon would have 14 internal stretching modes and hypothesizes that the seven or eight complex bands which lie between 650 and 1200 cm^{-1} are internal modes of this ribbon. The vibrations below 650 cm^{-1} belong to deformations of the AlO_6^{-9} octahedra.

Garnets (pyrope, grossular, and andradite). The compositions of the three garnets analyzed are given in Table 5. Spectra of a number of garnets have been published by *Moore et al.* [1971] and of almandine-pyrope by *Omori* [1971*b*]. Assignments of Raman modes, made by *Moore et al.* [1971] from polarization data obtained from a single crystal of Gr-90, provide a guide to the relative frequencies of stretching and bending modes. The w_1 and w_3 stretching modes occur above 695 cm^{-1}, w_2 and w_4 modes between 516 and 662 cm^{-1}, rotary (tetrahedral rocking) modes between 378 and 483 cm^{-1}, and translational modes below 348 cm^{-1}. The work of *Moore et al.* [1971] demonstrates that although the frequencies of many of the bands change systematically with composition and with cell parameters, they are not necessarily present in all spectra. In general, the lines found in the spectra of Figure 1*c* agree with those of *Moore et al.* [1971; Table 2, p. 58].

Calcite. The internal modes of the carbonate ion are well separated from the external modes: w_3, antisymmetric stretching at 1432 cm^{-1}; w_1, symmetric stretching at 1097 cm^{-1}; w_2, out-of-plane bending at 879 cm^{-1}; and w_4, in-plane bending at 714 cm^{-1} [*Cifrulak*, 1970]. The external modes lie in a narrow range between 398 and 92 cm^{-1}. Complete analysis of modes is given by *White* [1974].

NOTATION

c	speed of light.
C_V	heat capacity.
$\mathbf{K}$	wave vector.
$\mathbf{K}_{max}$	wave vector at Brillouin zone boundary.
q	fraction of vibrational modes which are internal stretching modes of molecular clusters (Table 6).
w	wave number, cm^{-1}.
θ_{el}	elastic Debye temperature.
ν	frequency, cycles per second or terahertz.
ω	frequency, radians per second.
ω_D	Debye cutoff frequency.

Acknowledgments. The far-infrared spectra reported here were obtained by the author in the laboratory of George Rossman, California Institute of Technology. Bob Jones (UCLA) provided microprobe analyses of the garnets, and Joan Delany (UCLA) provided X ray diffraction patterns of the minerals. The help of these people is gratefully acknowledged.

REFERENCES

Anderson, O. L., The Debye temperature of vitreous silica, *Phys. Chem. Solids, 12,* 41–52, 1959.

Barker, A. S., Infrared lattice vibrations and dielectric dispersion in corundum, *Phys. Rev. B, 132*(4), 1474–1481, 1963.

Born, M., and K. Huang, *Dynamical Theory of Crystal Lattices,* 429 pp., Oxford University Press, New York, 1954.

Bragg, L., G. F. Claringbull, and L. H. Taylor, *Crystal Structure of Minerals,* 409 pp., Cornell University Press, New York, 1965.

Buchanan, R. A., H. T. Caspers, and J. Murphy, Lattice vibration spectra of $Mg(OH)_2$ and $Ca(OH)_2$, *Appl. Opt., 2*(11), 1147–1150, 1963.

Cifrulak, S. D., High pressure mid-infrared studies of calcium carbonate, *Amer. Mineral., 55,* 815–824, 1970.

Clark, A. E., and R. E. Strakna, The low-temperature excess specific heat of SiO_2 glass, *Phys. Chem. Glasses, 3*(4), 121–126, 1962.

Cowley, E. R., and A. K. Pant, Lattice dynamics of calcite, *Phys. Rev. B., 8,* 4795–4800, 1973.

Dawson, P., M. M. Hargreave, and G. R. Wilkinson, The vibrational spectrum of zircon, *J. Phys. C, 4,* 240–256, 1971.

Dawson, P., C. D. Hadfield, and G. R. Wilkinson, The polarized infrared and Raman spectra of $Mg(OH)_2$ and $Ca(OH)_2$, *J. Phys. Chem. Solids, 34,* 1217–1225, 1973.

Elcombe, M. H., Some aspects of the lattice dynamics of quartz, *Proc. Phys. Soc. London, 91,* 947–958, 1967.

Farmer, V. C. (Ed.), *The Infrared Spectra of Minerals, Monogr. 4,* 539 pp., Mineralogical Society, London, 1974*a*.

Farmer, V. C., Vibrational spectroscopy in mineral chemistry, in *The Infrared Spectra of Minerals, Monogr. 4,* edited by V. C. Farmer, pp. 1–10, Mineralogical Society, London, 1974*b*.

Farmer, V. C., The layer silicates, in *The Infrared Spectra of Minerals, Monogr. 4,* edited by V. C. Farmer, pp. 331–363, Mineralogical Society, London, 1974*c*.

Farmer, V. C., Orthosilicates, pyrosilicates, and other finite chain silicates, in *The Infrared Spectra of Minerals, Monogr. 4,* edited by V. C. Farmer, pp. 285–303, Mineralogical Society, London, 1974*d*.

Farmer, V. C., The anhydrous oxide minerals, in *The Infrared Spectra of Minerals, Monogr. 4,* edited by V. C. Farmer, pp. 183–204, Mineralogical Society, London, 1974*e*.

Flubacher, P., A. J. Leadbetter, J. A. Morrison, and B. P. Stoicheff, The low-temperature heat capacity and the Raman and Brillouin spectra of vitreous silica, *J. Phys. Chem. Solids, 12,* 53–65, 1959.

Fraas, L. M., and J. E. Moore, Raman selection rule violation for a spinel crystal, *Rev. Brasil. Fis., 2*(3), 299–310, 1972.

Fraas, L. M., J. E. Moore, and J. B. Salzberg, Raman characterization studies of synthetic and natural $MgAl_2O_4$ crystals, *J. Chem. Phys., 58,* 3585–3592, 1973.

Griffith, W. P., Raman studies on rock-forming minerals, 1, Orthosilicates and cyclosilicates, *J. Chem. Soc. A,* 1372–1377, 1969*a*.

Griffith, W. P., Raman spectroscopy of minerals, *Nature, 224*(5216), 264–266, 1969*b*.

Hadni, A., The interaction of infrared radiation with crystals, in *The Infrared Spectra of Minerals, Monogr. 4,* edited by V. C. Farmer, pp. 11–26, Mineralogical Society, London, 1974.

Herzberg, G., *Infra-Red and Raman Spectra of Polyatomic Molecules,* 632 pp., Van Nostrand, New York, 1945.

Holm, J. L., O. L. Kleppa, and E. F. Westrum, Jr., Thermodynamics of polymorphic transformations in silica: Thermal properties from 5 to 1070°K and pressure-temperature stability fields for coesite and stishovite, *Geochim. Cosmochim. Acta, 31,* 2289–2307, 1967.

Hunt, J. M., M. P. Wisherd, and L. C. Bonham, Infrared absorption spectra of minerals and other inorganic compounds, *Anal. Chem., 22,* 1478–1497, 1950.

Iiishi, K., T. Tomisaka, T. Kato, and Y. Umegaki, Isomorphous substitution and infrared and far infrared spectra of the feldspar group, *Neues Jahrb. Mineral. Abh., 115*(1), 98–119, 1971.

Ishii, M., T. Shimanouchi, and M. Nakahira, Far infrared absorption spectra of layer silicates, *Inorg. Chim. Acta, 1,* 387–392, 1967.

Karr, C., Jr., *Infrared and Raman Spectroscopy of Lunar and Terrestrial Minerals,* 375 pp., Academic, New York, 1975.

Keller, W. D., J. H. Spotts, and D. L. Biggs, Infrared spectra of some rock-forming minerals, *Amer. J. Sci., 250,* 453–471, 1952.

Kieffer, S. W., I, Shock metamorphism of the Coconino sandstone at Meteor Crater, Arizona: II, The specific heat of solids of geophysical interest, Ph.D. thesis, 253 pp., Calif. Inst. of Technol., Pasadena, 1971.

Kieffer, S. W., Thermodynamics and lattice vibrations of minerals, 1, Mineral heat capacities and their relationships to simple lattice vibrational models, *Rev. Geophys. Space Phys., 17,* this issue, 1979*a*.

Kieffer, S. W., Thermodynamics and lattice vibrations of minerals, 3, Lattice dynamics and an approximation for minerals with application to simple substances and framework silicates, *Rev. Geophys. Space Phys., 17,* this issue, 1979*b*.

Kolesova, V. A., Infrared absorption spectra of the silicates containing aluminum and of certain crystalline aluminates, *Opt. Spectrosc. USSR,* Engl. Transl., *6,* 20–24, 1959.

Kovach, J. J., A. L. Hiser and C. Karr, Jr., Far-infrared spectroscopy of minerals, in *Infrared and Raman Spectroscopy of Lunar and Terrestrial Minerals,* edited by C. Karr, Jr., pp. 231–254, Academic, New York, 1975.

Launer, P. J., Regularities in the infrared absorption spectra of silicate minerals, *Amer. Mineral., 37,* 764–784, 1952.

Lazarev, A. N., *Vibrational Spectra and Structure of Silicates,* translated from Russian, 302 pp., Consultants Bureau, New York, 1972.

Leadbetter, A. J., The thermal properties of glasses at low temperatures, *Phys. Chem. Glasses, 9,* 1–13, 1968.

Leadbetter, A. J., Inelastic cold neutron scattering from different forms of silica, *J. Chem. Phys., 51,* 779–786, 1969.

Liese, H. C., Selected terrestrial minerals and their infrared absorption spectral data (4000–300 cm^{-1}), in *Infrared and Raman Spectroscopy of Lunar and Terrestrial Minerals,* edited by C. Karr, Jr., pp. 197–230, Academic, New York, 1975.

Lord, R. C., and J. C. Morrow, Calculation of the heat capacity of α-quartz and vitreous silica from spectroscopic data, *J. Chem. Phys., 26,* 230–232, 1957.

Lyon, R. J. P., Infra-red confirmation of six-fold co-ordination of silicon in stishovite, *Nature, 196,* 266–267, 1962.

Matossi, F., Frequency formulas for some atomic groups occurring in silicates, *J. Chem. Phys., 17,* 679–685, 1949.

Matossi, F., The vibration spectrum of rutile, *J. Chem. Phys., 19,* 1543–1546, 1951.

Mecke, R., Experimentelle Ergebnisse und Ziele der Bandenforschung, *Z. Elektrochem., 36,* 589–596, 1930*a*.

Mecke, R., Das Rotationsschwingungsspektrum des Acetylens, III, Die Eigenfrequenzen einfacher symmetrischer Moleküle, *Z. Phys., 64,* 173–185, 1930*b*.

Moenke, H. H. W., *Mineralspektren,* parts I and II, Akademie, Berlin, 1962.

Moenke, H. H. W., Vibrational spectra and the crystal-chemical classification of minerals, in *The Infrared Spectra of Minerals, Monogr. 4,* edited by V. C. Farmer, pp. 111–118, Mineralogical Society, London, 1974.

Moore, R. K., W. B. White, and T. V. Long, Vibrational spectra of the common silicates, I, The garnets, *Amer. Mineral., 56,* 54–71, 1971.

Neuberger, J., and R. D. Hatcher, Infrared optical constants of NaCl, *J. Chem. Phys., 34,* 1733, 1961.

Oehler, O., and H. H. Günthard, Low temperature infrared spectra between 1200 and 20 cm^{-1} and normal coordinate analysis of silicates with olivine structure, *J. Chem. Phys., 51,* 4719–4728, 1969.

Omori, K., Analysis of the infrared absorption spectrum of diopside, *Amer. Mineral., 56,* 1607–1616, 1971*a*.

Omori, K., Analysis of the infrared absorption spectrum of almandine-pyrope garnet from Nijosan, Osaka prefecture, Japan, *Amer. Mineral., 56,* 841–849, 1971*b*.

Pandey, H. N., The theoretical elastic constants and specific heats of rutile, *Phys. Status solidi, 11,* 743–751, 1965.

Porto, S. P., and R. S. Krishnan, Raman effect of corundum, *J. Chem. Phys., 47*(3), 1009–1012, 1967.

Porto, S. P., P. A. Feury, and T. C. Damen, Raman spectra of TiO_2, MgF_2, ZnF_2, FeF_2 and MnF_2, *Phys. Rev., 154,* 522–526, 1967.

Preudhomme, J., and P. Tarte, Infrared spectra of spinels, I, A critical discussion of the actual interpretation, *Spectrochim. Acta, Part A, 27,* 961–968, 1971*a*.

Preudhomme, J., and P. Tarte, Infrared spectra of spinels, II, The experimental bases for solving the assignment problem, *Spectrochim. Acta, Part A, 27,* 845–851, 1971*b*.

Preudhomme, J., and P. Tarte, Infrared spectra of spinels, III, The normal II-III spinels, *Spectrochim. Acta, Part A, 27,* 1817–1835, 1971*c*.

Preudhomme, J., and P. Tarte, Infrared studies of spinels, IV, Normal spinels with a high valency cation, *Spectrochim. Acta, Part A, 28*, 69–79, 1972.

Raunio, G., L. Almquist, and R. Stedman, Phonon dispersion relations in NaCl, *Phys. Rev., 178*, 1496–1501, 1969.

Safford, G., V. Brajovic, and H. Boutin, An investigation of the energy levels in alkaline earth hydroxides by inelastic scattering of slow neutrons, *Phys. Chem. Solids, 24*, 771–777, 1963.

Saksena, B. D., Analysis of the Raman and infrared spectra of α-quartz, *Proc. Indian Acad. Sci., Sect. A, 12*, 93–137, 1940.

Saksena, B. D., Force constants and normal modes of the totally symmetric vibrations in α-quartz at room temperature, *Proc. Indian Acad. Sci., Sect. A, 16*, 270–277, 1942.

Saksena, B. D., Calculation of the infra-red active and Raman inactive frequencies of α-quartz, *Proc. Indian Acad. Sci., Sect. A, 22*, 379–382, 1945.

Saksena, B. D., Infra-red absorption studies of some silicate structures, *Trans. Faraday Soc., 57*, 242, 1961.

Sangster, M. J. L., G. Peckham, and D. H. Saunderson, Lattice dynamics of magnesium oxide, *J. Phys. C, 3*, 1026–1036, 1970.

Scheetz, B. E., and W. B. White, Vibrational spectra of the alkaline earth double carbonates, *Amer. Mineral., 62*, 36–50, 1977.

Scott, J. F., and S. P. S. Porto, Longitudinal and transverse optical lattice vibrations in quartz, *Phys. Rev., 161*, 903–910, 1966.

Simon, I., and H. O. McMahon, Study of the structure of quartz, cristobalite and vitreous silica by reflection in infrared, *J. Chem. Phys., 21*, 23–30, 1953.

Tarte, P., Study of silicates by infrared spectrometry; present results and future prospects, *Bull. Soc. Fr. Ceram., 58*, 13–34, 1963.

Traylor, J. G., H. G. Smith, R. M. Nicklow, and M. K. Wilkinson, Lattice dynamics of rutile, *Phys. Rev. B, 3*(10), 3457–3472, 1971.

Venkataraman, G., and V. C. Sahni, External vibrations in complex crystals, *Rev. Mod. Phys., 42*(4), 409–470, 1970.

White, W. B., The carbonate minerals, in *The Infrared Spectra of Minerals, Monogr. 4*, edited by V. C. Farmer, pp. 227–284, Mineralogical Society, London, 1974.

White, W. B., Structural interpretation of lunar and terrestrial minerals by Raman spectroscopy, in *Infrared and Raman Spectroscopy of Lunar and Terrestrial Minerals*, edited by C. Karr, Jr., pp. 325–358, Academic, New York, 1975.

White, W. B., and B. H. De Angelis, Interpretation of the vibrational spectra of spinels, *Spectrochim. Acta, Part A, 23*, 985–995, 1967.

(Received May 24, 1978;
accepted August 28, 1978.)